Atmospheric Research 158–159 (2015) 274–291

Contents lists available at ScienceDirect

Atmospheric Research

journal homepage: www.elsevier.com/locate/atmos

Invited review article

A review of supercell and tornado dynamics

Robert Davies-Jones *

Emeritus, NOAA National Severe Storms Laboratory, Norman, OK, USA

ARTICLE INFO

Article history:
Received 29 November 2013
Received in revised form 1 April 2014
Accepted 4 April 2014
Available online 16 April 2014

Keywords:
Supercells
Tornadoes
Tornadogenesis
Mesocyclone
Helicity

ABSTRACT

Thunderstorms that form in strong vertical wind shear often evolve into supercell storms. Supercells are well-organized, monolithic units of vigorous long-lasting convection. A classic supercell in its mature stage consists of a rotating updraft (mid-altitude mesocyclone) and a downdraft that coexists symbiotically with the updraft in an almost steady state.

Doppler-radar and visual observations along with computer simulations reveal that tornadic supercells evolve through three stages. Firstly, the updraft starts rotating and a mesocyclone forms aloft, secondly a narrower vortex develops near the ground (thus completing a rotating column that extends from the ground to upper levels), and lastly a tornado forms from contraction of the near-ground cyclone.

The updraft tilts environmental horizontal vorticity upwards. The updraft rotates cyclonically as a whole if this vorticity is streamwise in the updrafts' reference frame (i.e., in the direction of the storm-relative wind). Updraft rotation and motion are linked so a complete theory of mid-altitude mesocyclones requires an understanding of how supercells propagate. There are two principle propagation mechanisms; one is linear and the other is nonlinear.

The process whereby rotation develops in rising air cannot explain how cyclonic rotation starts near the ground where updrafts and background vertical vorticity are normally weak. A near-ground cyclone does not form without a downdraft. In computer simulations, low-altitude air parcels with cyclonic vorticity have previously subsided in horizontal gradients of buoyancy that generate horizontal vorticity. During an air parcel's descent, its horizontal vorticity is first tipped downward into anticyclonic vorticity, but then upwards into cyclonic vorticity before it reaches the nadir of its trajectory because the vorticity vector is inclined upward relative to the velocity vector. The parcel then flows close to the ground into the updraft where its cyclonic vorticity is greatly amplified as it is stretched vertically.

In simulations, this near-ground cyclone collapses into a tornado only if the model includes surface friction, which paradoxically causes the extreme upward and rotary winds. With friction, inflowing air parcels near the ground penetrate much closer to the rotation axis and revolve much faster despite some loss of angular momentum to the ground. Their extra kinetic energy comes from a further loss in their enthalpy.

Published by Elsevier B.V.

Contents

* Doggetts Farm, New Street, Stradbroke, Eye, Suffolk, IP 21 5JG, U.K. Tel.: +44 1379 384869.
E-mail address: bobdj1066@yahoo.com.

http://dx.doi.org/10.1016/j.atmosres.2014.04.007
0169-8095/Published by Elsevier B.V.

1. Introduction

In environments with convective available potential energy (CAPE) and ground-relative winds that turn and increase markedly with height, thunderstorms can evolve into vigorous and highly organized units of convection known as supercells. Despite ordinary cells being far more common, supercells are responsible for much of the violent weather that occurs (tornadoes, destructive straight-line winds, and large hail). Almost all strong tornadoes are associated with supercells, and most of them happen in environments with strong shear. The structure of a typical supercell storm is depicted in Figs. 1 and 2. A supercell is a large, quasi-steady, unicellular, propagating storm with a rotating updraft. In the northern hemisphere[1] (the viewpoint adopted here), most supercells have a cyclonically rotating updraft that moves or propagates to the right side of the environmental-wind hodograph curve (Bluestein, 2013, pp. 216 ff.). The cyclonically rotating region of a right-moving (RM) supercell is a mesocyclone. A few supercells move leftward and have a mesoanticyclone (which is primarily an anticyclonically rotating updraft). These left-moving (LM) storms can be notorious hail producers, but rarely create tornadoes.

The genesis of the first tornado in a supercell is a complicated process that generally takes over an hour after storm initiation. The tornado is generally preceded by a near-ground cyclone that is intermediate in size between a mesocyclone and a tornado. Tornadogenesis in supercells seems to occur in three stages:

Stage 1 Formation of a rotating updraft aloft.
Stage 2 Development of a cyclone at the ground.[2]
Stage 3 Formation of the tornado (collapse and spin-up of the above cyclone).

[1] For southern-hemisphere storms, left and right are interchanged.
[2] Technically winds at the ground vanish because of the no-slip condition. Ground in this article refers to the top of the laminar sublayer (millimeters above the ground) where significant winds do occur.

The three stages are described in Sections 2–4. Some supercell storms exhibit cyclic behavior with a series of cyclones that generate a succession of tornadoes. Subsequent cyclones form more quickly than the first one. For further details on this topic, the reader is referred to Adlerman et al. (1999) and Davies-Jones et al. (2001, pp. 192–195). Section 3.2 includes a new perception of the baroclinic mechanism. Section 4 also gives reasons why tornadogenesis sometimes fails when a tornado is about to happen (within a few minutes). The diverse structures of tornado vortices and tornado decay are described in Section 5. The dynamics of tornadoes and the reason why they are so powerful are summarized in Section 6. The reviews by Davies-Jones (1986), Lewellen (1993), Davies-Jones et al. (2001), Markowski and Richardson (2010), Bluestein (2013) and Rotunno (2013) contain additional topics and more details.

2. Stage 1 of tornadogenesis: the mid-altitude mesocyclone

Since 1971, Doppler radar observations have shown that mesocyclones form aloft first and then near the ground prior to tornadogenesis (Burgess and Lemon, 1990). The circulation (line integral of tangential wind) around a mesocyclone aloft is roughly 2 to 6 $\times$ 10^5 m^2 s^{-1}, based on a typical maximum tangential wind of 21 m s^{-1} at a radial distance from the circulation center of 1.5 to 4.5 km.

The mesocyclone aloft is a consequence of the updraft tilting up horizontal streamwise vorticity present in the storm's inflow (Lilly, 1982; Davies-Jones, 1984). The resulting vertical vorticity is then amplified by vertical stretching in the lower part of the updraft and transported upward in the rising air, thereby extending the mesocyclone to anvil height in some cases. The component of horizontal vorticity parallel to the air stream is not Galilean invariant; it is different, for example, in ground-relative and storm-relative frames of reference. The updraft is doing the tilting and so *updraft-relative* streamwise vorticity is the physically relevant quantity. The theory is incomplete because the updraft motion is an unknown. In environments with strongly curved hodographs the process is quite insensitive to the exact storm motion

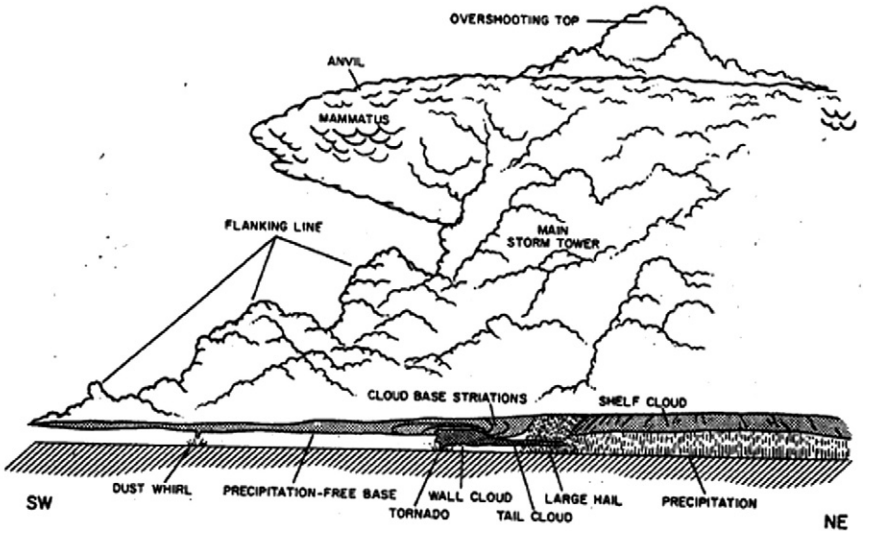

Fig. 1. Composite view of a tornadic supercell as viewed from the southeast. The horizontal scale is compressed. All the features cannot be seen at the same distance. Based on an original drawing by C. A. Doswell III.

because the storm-relative vorticity has a streamwise component for a wide range of feasible storm motions.

For forecasting mesocyclone formation and intensity, the storm-relative environmental helicity (SREH; Droegemeier et al., 1993) is evaluated (Davies-Jones et al., 1990) because compared to streamwise vorticity it is far less sensitive to measurement error and sampling resolution. The SREH is the integral over the inflow's vertical range (nominally 0 to 3 km) of the scalar product of the storm-relative inflow velocity and the horizontal vorticity. Inclusion of the inflow wind filters out cases where tornadogenesis is unlikely because the inflow is too weak to prevent the storm's rain-cooled outflow from surging far ahead of the storm (see Section 5). A hodograph is a plot of the environmental vector wind $\overline{\mathbf{v}}(z)$ on a (u, v) diagram where u and v are eastward and northward vector components, respectively (Fig. 3). The height z acts as the parameter of the hodograph curve. The tangent vector $d\overline{\mathbf{v}}/dz$ is the environmental shear $\mathbf{S}(z)$ and the environmental horizontal vorticity vector $\overline{\boldsymbol{\omega}}_H(z) \equiv \mathbf{k} \times \mathbf{S}(z)$ is 90° to its left ($\mathbf{k}$ is the unit vertical vector). Plotting the storm-motion vector $\mathbf{c}$ on the hodograph diagram and drawing wind arrows from it to the curve yields storm-relative wind $\overline{\mathbf{v}}(z)-\mathbf{c}$. The storm-relative streamwise vorticity is the component of $\overline{\boldsymbol{\omega}}_H(z)$ in the direction of the storm-relative wind. SREH is minus twice the area swept out counterclockwise by the storm-relative wind over the specified height range. It is easily computed for all feasible storm motions $\mathbf{c}$ so the forecaster can assess readily which of the observed storm motions are most favorable for mesocyclones. Forecasters also can assess visually the amount of SREH over the lowest kilometer. Large 0–1 km helicity is especially conducive to tornadoes (Markowski et al., 1998) because the base of the mesocyclone aloft is not far off the ground.

2.1. Updraft rotation in turning shear

We now present the linear theory, which explains how an incipient updraft rotates in the case when the storm-relative environmental wind $\overline{\mathbf{v}}(z)-\mathbf{c}$ veers with height without changing speed and thus has purely streamwise vorticity. Let Z be the original height of a parcel (i.e., far away from the updraft). This is conserved. Fig. 4 depicts the process at a fixed height $z_0 = 2$ km. For an axisymmetric updraft, the contours of Z in the diagram are roughly concentric circles with Z decreasing to a minimum at the center. The vertical displacement is $z_0 - Z$ and peaks at the center. The only horizontal force (aside from a small amount of friction) is the pressure-gradient force, which is irrotational. Therefore we can deduce the rotational part of the horizontal wind field by proceeding as if the horizontal momentum of each parcel is conserved. By transferring the storm-relative environmental winds at height Z to the Z-contours in Fig. 4, we find that the region upstream (downstream) of the peak vertical displacement is cyclonic (anticyclonic). We still have to deduce where the maximum updraft is relative to the peak. The vertical wind is $w = d(z_0-Z)/dt = -\partial Z/\partial t-(\overline{\mathbf{v}}-\mathbf{c})\cdot\nabla Z$ in the updraft's reference frame where t is time. Because the shape of $\partial Z/\partial t$ is roughly axisymmetric, the maximum vertical velocity occurs on the upstream side of the peak, which is also where the cyclonic vortex is located. The anticyclonic vortex is downstream of the peak in downdraft or weaker updraft. Thus, vertical velocity and vertical vorticity are correlated and the overall updraft rotation is cyclonic.

In the opposite case of purely crosswise vorticity where the storm-relative environmental wind increases speed with height with no change in direction (straight hodograph), the above procedure reveals that the right and left sides (looking downshear) of the updraft rotate cyclonically and anticyclonically, respectively, with no overall rotation. Updrafts in this case rotate as a whole only if their storm motion vector lies oddly off the hodograph curve.

2.2. Updraft propagation and rotation

In strong unidirectional shear from low to mid heights, initial storms split into right- and left-moving supercells. The

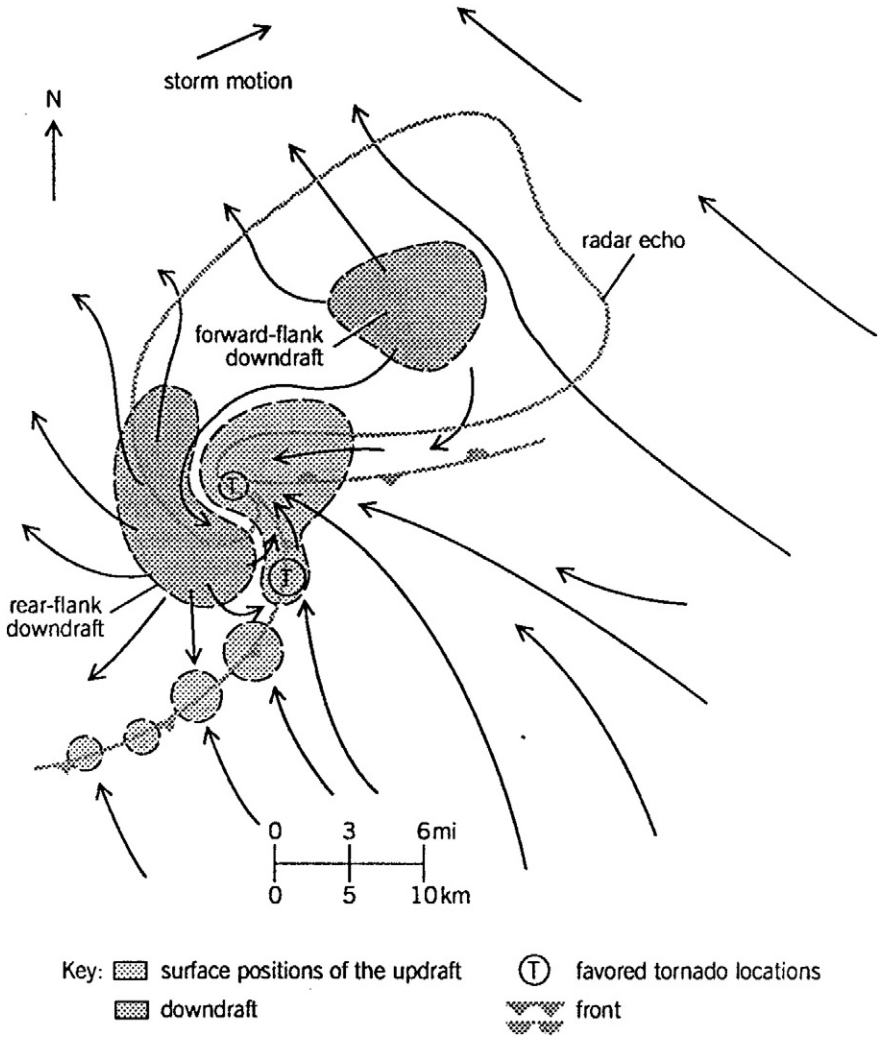

Fig. 2. Schematic surface plan view of a tornadic supercell. The thick line encompasses the low-elevation radar echo. The solid line with cold-frontal symbols marks the rear-flank gust front, and the one with stationary-front symbols outlines the less obvious forward-flank convergence boundary. Sometimes there is also a left-flank convergence boundary (not shown) that extends from the wave apex of the gust front towards the left flank (see Fig. 8 in Beck and Weiss, 2013). Low-altitude locations of the updraft are finely stippled; forward-flank downdraft (FFD) and rear-flank downdraft (RFD) are coarsely stippled. Streamlines are storm-relative. The northern encircled T at the wave apex of the gust front marks the most likely location of a major cyclonic tornado. The southern T at the bulge in the gust front is where a new mesocyclone and tornado may be developing. The south side of the RFD is where an anticyclonic tornado occasionally forms. From Davies-Jones (1986), based on an original drawing by C. Doswell.

environmental winds acting on a passive storm would tilt it but not cause it to move off the hodograph. The anomalous motion of the supercell updrafts to the right and left sides of the straight hodograph is due to propagation, which is the part of updraft motion attributed to the updraft actively growing on one side and decaying on the opposite side. The non-hydrostatic (NH) vertical pressure-gradient force (VPGF) is the part of the VPGF that is not balanced by the downward gravitational acceleration. At each level, supercell updrafts deviate from the environmental steering wind at that level by propagating towards (away from) the edge where the NHVPGF is upward (downward) (Rotunno and Klemp, 1982; Davies-Jones, 2002). The RM updraft gains cyclonic circulation at each level by propagating continuously into a markedly cyclonic region and away from an anticyclonic region, picking up strong cyclonic vorticity on its growth side and discarding anticyclonic or weak cyclonic vorticity on its decay side (Davies-Jones, 2004). The LM updraft does the opposite. This mechanism of updraft rotation is equivalent to the one in Section 2.1.

For a steady-state storm, the continuous propagation off the hodograph at each level has to be just right to yield a height-independent storm motion vector. The propagation vectors $\mathbf{P}(z)$ from the steering current $\bar{\mathbf{v}}(z)$ on the hodograph curve must all end up at $\mathbf{c}$ so that $\mathbf{P}(z) = \mathbf{c} - \bar{\mathbf{v}}(z)$. Qualitative understanding of propagation clearly requires knowing the factors that determine the locations of the maxima and minima of the NHVPGF field in each level.

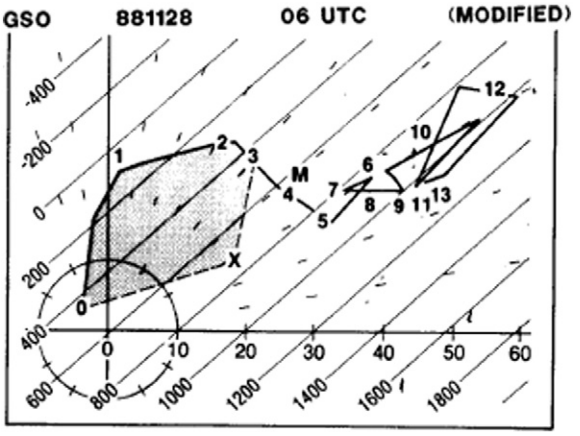

Fig. 3. Hodograph diagram for the environment of a violent tornado. Numbers along the hodograph curve denote height above the ground in km. The storm-motion vector **c** is from the origin to X. Vector from the origin (or X) to a point z on the curve is the ground- (or storm-) relative wind $\bar{\mathbf{v}}(z)-\mathbf{c}$ at height z. M marks the mean wind between the surface and 200 mb. The propagation vector, $\mathbf{P}(z)$, is from z to X. The SREH (in $m^2\ s^{-2}$) in the lowest 3 km is twice the shaded area. Straight lines parallel to 0–3 km shear vector are contours of SREH as a function of storm motion (location of X). From Davies-Jones et al. (1990).

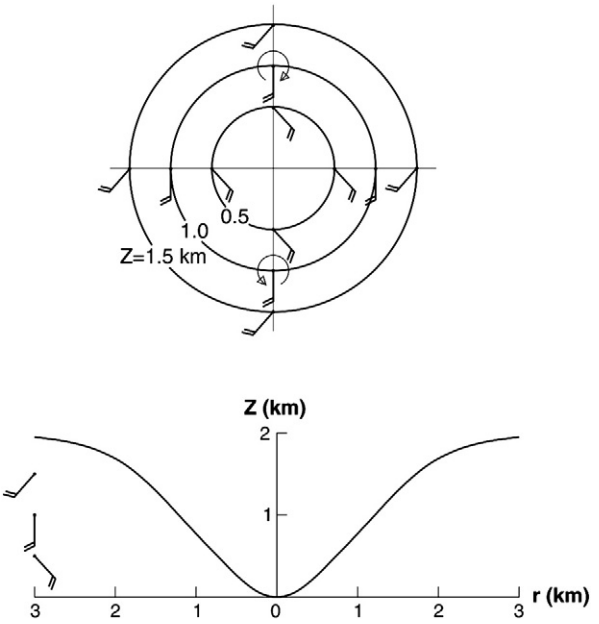

Fig. 4. How the updraft rotates when the environmental storm-relative winds veer with height. The level is at height $z_0 = 2$ km. The circles in the top panel are the contours of the heights Z of parcels when they were in the upstream environment. The contours are circular for simplicity. In the lower panel, the wind profile is shown on the left and the graph is for $Z(r)$ where r is the radial distance from the center of the Z field. The wind barbs in the top panel are the winds that would occur if the horizontal momentum of parcels were conserved. The wind pattern has cyclonic (curvature) vorticity on the upstream side of the peak in vertical displacement, $z_0 - Z$. This is also the side where the vertical velocity is largest so vertical velocity and vertical vorticity are correlated positively.

2.3. The nonhydrostatic pressure

The non-hydrostatic pressure p_{nh} is the solution of the Poisson equation,

$$-\nabla^2 p_{nh} = g\nabla_H^2 \mathcal{M} + 2\rho \mathbf{S}(z)\cdot\nabla_H w + \text{nonlinear splat} + \text{nonlinear spin} - \rho f\zeta \qquad (1)$$

obtained by taking the divergence of the equations of motion (Davies-Jones, 2002). The first term on the right is linear forcing due to horizontal variations in the weight $\mathcal{M}g$ of overlying air and water. The second term is linear forcing caused by the interaction between the updraft's horizontal gradient $\nabla_H w$ and the environmental wind shear $\mathbf{S}(z)$ (Rotunno and Klemp, 1982). The third and fourth terms are nonlinear dynamical forcing terms (Davies-Jones, 2002). The negative-definite spin term is minus the air density ρ times one half the squared magnitude of the deviation (from the environmental quantity at the same height) of vorticity and tends to force low pressure (as in vortices). The positive-definite splat term is ρ times the squared magnitude of the deviation rate-of-deformation tensor. It acts to force high pressure (as in highs at stagnation points). The last term is a small Coriolis term, in which f is the Coriolis parameter and ζ is vertical relative vorticity. Like the forcing in Eq. (1), the NHVPGF, $-\rho^{-1}\ \partial p_{nh}/\partial z$, and hence the propagation can be decomposed into mass-induced, shear-induced and nonlinear parts. Mass-induced propagation is generally small at 3 km, the level where the modelers typically have investigated propagation. Note however that cold pools do affect supercell propagation at lower altitudes.

2.4. Supercell propagation in unidirectional shear

In nearly or purely unidirectional strong shear the initial non-supercell storm splits into RM and LM supercells. Let the shear be westerly for example. The associated environmental vorticity is northward so the lifting of vorticity tubes by the initial updraft produces a cyclonic (anticyclonic) mid-altitude vortex on its south (north) side.

The storm splits as a result of two effects. First, precipitation that accumulates along its west–east axis exerts downward drag on the air, turns updraft into downdraft there, and causes the original maximum to disappear (Klemp and Wilhelmson, 1978). Even though simulated storms split without precipitation (Rotunno and Klemp, 1982), this effect accelerates the splitting process. Second, the vortices are low-pressure centers, and the upward pressure-gradient force beneath them promotes new updraft growth. Thus, the supercell to the south (north) propagates towards the right (left) into the vortex on that side, thereby picking up cyclonic (anticyclonic) vorticity. Updraft propagation in both supercells depends on the nonlinear spin part of the forcing in Eq. (1) (Rotunno and Klemp, 1985), and arises only indirectly from the updraft-shear interaction. In simulations with unidirectional shear and no Coriolis force, the two supercells are mirror images of one other. The Coriolis term in Eq. (1) increases the magnitude of the spin forcing in the RM rotating updraft and reduces it in the LM updraft. Consequently, the RM supercell is slightly stronger than the LM one when the Coriolis force is included in the simulation (Klemp and Wilhelmson, 1978).

2.5. Supercell propagation in turning shear

Veering (clockwise turning) with height of the low-altitude shear vector enhances the RM updraft and suppresses the LM updraft to a much greater degree than the Earth's spin does (Klemp and Wilhelmson, 1978). As the hodograph curvature increases, splitting becomes insignificant and the left moving products of splitting are short lived (Klemp, 1987). Even though the nonlinear NHVPGF has greater amplitude than the linear NHVPGF, its maximum is centered almost on the updraft maximum while the linear NHVPGF has a positive–negative (upward–downward) couplet straddling the updraft. Consequently, linear propagation, which arises directly from the updraft–shear interaction, dominates nonlinear propagation. In environments with circular hodographs, the highs and lows of shear-induced pressure twist with height around the updraft in such a way that the resulting linear NHVPGF causes propagation to the concave side of the hodograph curve (Davies-Jones, 2002).

2.6. Stage 1 summary

During stage 1, a mesocyclone forms aloft as a result of the updraft tilting large storm-relative streamwise vorticity that is present in the storm inflow. For this to happen, the motion vector must lie significantly to the right of the hodograph curve, and the quasi-steady supercell updraft has to propagate strongly [since the propagation vector $\mathbf{P}(z) \equiv \mathbf{c} - \overline{\mathbf{v}}(z)$].

3. Stage 2 of tornadogenesis: rotation at ground

The next stage is the development of rotation next to the ground. Winds near the ground intensify rapidly as this happens. The mechanism is a lot different from the procedure for mid-altitude mesocyclone genesis. Before describing it, we need to introduce a logical partition of vorticity and circulation into barotropic, baroclinic and frictional parts (Dutton, 1986; Epifanio and Durran, 2002; Davies-Jones, 2006). The vorticity and circulation associated with the Earth's rotation are included in the barotropic parts. The division is not unique because it depends on the choice of an arbitrary starting time. This choice often is dictated by data availability and accuracy issues such as error growth in trajectory calculations.

Consider a parcel that is initially spherical. The barotropic vorticity of the parcel at a current time is determined only by its initial vorticity and its current deformation. Note that it is independent of its deformation history. Barotropic vortex tubes are frozen into the fluid (i.e., they always consist of the same material parcels).

The baroclinic vorticity of a parcel is zero initially, and at any current time depends primarily on its time-integrated buoyancy history and its deformation history since the initial time. The buoyancy force is

$$b\mathbf{k} \equiv -g\left(\frac{\rho'}{\rho} + q\right)\mathbf{k} \tag{2}$$

where g is the gravitational acceleration, ρ' is the density perturbation and gq is the weight of hydrometeors per unit mass of air.

A spherical parcel that is more buoyant on one side spins about a horizontal axis with the vorticity directed to the right of the buoyancy gradient. Thus, baroclinic vorticity is generated horizontally by horizontal gradients of the buoyancy force. If we divide the time between the initial time and the present into many tiny intervals, the baroclinic vorticity generated in each subinterval is bought forward to the present by being frozen to the material fluid. The frictional vorticity of a parcel is also zero initially. It is similar to the baroclinic vorticity, but depends on the accumulated effects of the curl of the friction force (rather than the time integral of the buoyancy curl).

Absolute circulation also can be decomposed into barotropic, baroclinic and frictional parts. Around a material circuit $C(\tau)$, the absolute circulation $\Gamma(\tau^*)$ at the present time τ^* is

$$\Gamma(\tau*) = \Gamma(\tau_0) + \int_{\tau_0}^{\tau*} A(\tau)d\tau + \int_{\tau_0}^{\tau*}\left[\oint_{C(\tau)} \mathbf{F}(\tau)\cdot d\mathbf{s}\right]d\tau \tag{3}$$

where τ is the time, τ_0 is the initial time, $\mathbf{F}$ is the friction force, $\mathbf{ds}$ is the vector increment of length along $C(\tau)$, and $A(\tau)$ is defined by

$$A(\tau) \equiv -\oint_{C(\tau)} \alpha dp \approx \oint_{C(\tau)} b(\tau)dz \tag{4}$$

in which p is the pressure and $\alpha \equiv \rho^{-1}(1+q)^{-1}$ is the reciprocal of the density of the air-water system. The right side of Eq. (4) is not a good approximation to A very close to a tornado because perturbations from a horizontally uniform basic state are large there. The first term on the right side of Eq. (3) is the barotropic circulation Γ_{BT}. It depends only on the initial time τ_0 because it is conserved by Kelvin's circulation theorem. The second and third terms are the baroclinic circulation Γ_{BC} and the frictional circulation Γ_{FR}, respectively. Both are zero initially. Results depend naturally on $\tau^*-\tau_0$. If this interval is small, then obviously the circulation is mostly barotropic. The frictional circulation has not been calculated directly, but may be significant for circuits that are close to the ground in the atmosphere and in simulations with surface friction, as well as for circuits that pass through regions where the subgrid-scale eddy stress terms in the momentum equations are large.

3.1. The need for a downdraft

Tilting by an updraft of horizontal vorticity fails to produce rotation next to the ground because the vertical vorticity is generated as the air is rising to hundreds of meters above the ground. Furthermore, the baroclinic circulation term in Eq. (3) around a horizontal material curve on flat ground is small (compared to a tornado's circulation) on the thunderstorm scale over a time interval of an hour or two. This is a consistent with the insignificance of the solenoidal term in the vertical-vorticity equation. Therefore, tornadogenesis must await the development of downdrafts (Davies-Jones, 1982a,b). This statement would be disproved if there were a way that substantial near-ground rotation could develop in a flow without a downdraft. There are three possibilities.

The first idea is that near-ground rotation develops from concentration of weak background vertical vorticity associated with the Earth's rotation and large-scale weather systems. Even though Coriolis forces are insignificant on the scale of individual thunderstorms, we cannot dismiss this hypothesis based

on theory. In the Appendix we derive and use a formula for the time that a persistent updraft of finite radius would take to concentrate Earth's rotation into a strong vortex. The estimated formation time for a strong tornado of 83 min obtained in the Appendix roughly agrees with times that simulated supercells take to develop significant near-ground rotation. For an observed large tornado cyclone the computed time is too long (Appendix). Replacing the Coriolis parameter f with a significantly larger environmental background vertical vorticity $\zeta_0 + f$ would result of course in shorter formation times. However, in supercell environments the background vertical vorticity is insignificant to low-level horizontal vorticity, which can be 50 times f (Davies-Jones, 1984). Thus, tilting of horizontal vorticity by the updraft, which quickly gives rise to mid-level updraft rotation (Section 2), could set the stage for a faster tornadogenesis mechanism involving downdrafts.

Furthermore, there is convincing numerical-modeling and observational evidence counter to the theory that the rotation of supercell tornadoes derives directly from the Earth's rotation or other background vorticity. Most importantly, computer simulations reproduce the observed features of classic supercells, including tornado-like vortices, with Coriolis forces deactivated and without any background vertical vorticity. Moreover, Doppler radar and visual observations show that the cyclonic tornado does not form in the middle of the updraft as might be expected based on the theory, but on one side with a downdraft nearby. The theory also is incapable of explaining why there is anticyclonic vorticity in close proximity to the cyclonic tornado and why an anticyclonic tornado occasionally forms only a few kilometers away. A downdraft is needed to account for these observations.

The second possible process for developing near-ground rotation without a downdraft is by air parcels and vortex tubes being turned up abruptly into the vertical at a gust front (Simpson, 1982). However, Davies-Jones and Markowski (2013) used a two-dimensional, but three-directional, simulation to show that such abrupt turning does not happen. The flow ahead of the gust front resembles a stagnation flow with high pressure at the front. The approaching air decelerates rapidly in the adverse pressure gradient, and starts rising before it reaches the gust front. Thus, the tilting of vortex tubes is not abrupt. More importantly, the horizontal vorticity available for tilting is greatly reduced by horizontal shrinking prior to its tilting.

The third hypothetical mechanism is by air parcels and vortex tubes being turned up abruptly through the dynamic-pipe effect (Smith and Leslie, 1978; Trapp and Davies-Jones, 1997). The core of a vortex is in stable cyclostrophic equilibrium, meaning that there is a balance of forces in the radial direction between the inward pressure-gradient and outward centrifugal forces and that parcels displaced radially experience a net restoring force. Thus the wall of a vortex core is impenetrable to outside air. The wall acts dynamically as a vertical pipe with suction (low pressure) because air enters it from below, not through the side. The core builds downwards if inflowing air has angular momentum because then it spins up as it converges on the entrance, and adds itself to the vortex. As the vortex continuously approaches the ground in this manner, air accelerates along the surface towards the low pressure in the core and turns suddenly upwards. However, there is a Catch-22 (stalemate): the sharp turn in the streamlines depends on the dynamic-pipe effect, which works only when the air near the ground already has considerable angular momentum. We should also note that rotation still develops next to the ground in supercell simulations with grids that are too coarse to resolve abrupt turning. Furthermore, there is no evidence that the mesocyclone aloft builds downwards all the way to the surface through the dynamic-pipe effect. Instead, it appears that a near-ground vortex forms by a different process. When the near-ground cyclone moves underneath the mesocyclone, a continuous wide vortex column is completed from the ground to upper levels of the storm.

3.2. Baroclinic mechanism

In computer models, rotation near the ground develops though tilting of horizontal vorticity, which is generated baroclinically in subsiding air that has spent 15 min or longer in a horizontal buoyancy gradient (Rotunno and Klemp, 1985). The vorticity in this air changes from anticyclonic to cyclonic during its descent because the vorticity vector is inclined upward relative to the velocity vector (Davies-Jones and Brooks, 1993; Davies-Jones et al., 2001). Its cyclonic vorticity is then greatly amplified by vertical stretching as it passes into the updraft. In simulations without surface friction, rotation just above the ground stems primarily from the baroclinic process, although it may be aided sometimes by barotropic circulation if the hodograph is extremely curved at low levels (Wicker and Wilhelmson, 1995).

Prior to the field experiment VORTEX1 in 1994 and 1995, researchers thought that the vorticity maximum near the ground should be located in strong gradients of temperature (T) and moist entropy. This belief was based on the results of numerical supercell simulations, which we now know overdid the baroclinic process owing to their microphysics parameterizations. The models produced too much rain too low in the cloud too soon, and evaporation was too fast, resulting in excessive cooling of the air (Straka and Rasmussen, 1997). All this led to a strong cold pool occurring too early in a storm's lifetime. Unexpectedly, field observations obtained during VORTEX1 and subsequent experiments did not find very cool air with low moist entropy at 3 m above the ground near strong and violent tornadoes (Markowski, 2002a; Markowski et al., 2002). These tornadoes were located only in modest temperature and entropy gradients, while strong temperature gradients sustained only weak tornadoes. The back-of-the-envelope calculation below explains how enough circulation can be generated baroclinically with only minor temperature differences.

The origin of near-surface circulation in simulated and observed storms is determined by drawing a small horizontal closed curve around the vorticity maximum at time τ^* and using backwards parcel trajectories to trace the past whereabouts of the material circuit to some initial time τ_0 (Rotunno and Klemp, 1985; Davies-Jones and Brooks, 1993) when it is typically large and convoluted. The circulation at τ^* equals the initial or barotropic circulation plus circulation generated baroclinically and by friction during the interval (τ_0, τ^*) according to Eq. (3). Calculation of baroclinic circulation is sensitive to the accuracy of the divergent backward trajectories. In particular, there should not be obvious errors such as

parcels crossing an air-mass boundary into a region where they clearly don't belong (Dahl et al., 2012).

Note that $A(\tau)$ in Eq. (4) is a signed area in (b, z) space or, more generally, in (p, α) space. Thus, there is a large baroclinic circulation if and only if there has been a large area in (b, z) space for a long time. This area becomes small during the last few minutes before τ^* as the circuit flattens out and its height increment dz tends to zero. Most of the baroclinic circulation is generated at earlier times in higher-altitude parts of the circuit. Therefore, the relevant baroclinic zone is slightly aloft and perhaps in a quite different part of the storm than the vorticity maximum. Also note that the baroclinic zone does not have to be narrow because the size of the baroclinic circulation depends on horizontal differences in buoyancy, and not on the magnitude of horizontal buoyancy gradients. Baroclinic generation of horizontal vorticity is proportional to the size of buoyancy gradients, leading to the belief that the baroclinic mechanism relies on parcels spending long times in strong thermal gradients. However, vorticity can magnify from small seeds of baroclinic generation as the circuit contracts greatly.

The amount of baroclinic circulation may be estimated as

$$\Gamma_{BC} = (\tau * - \tau_0)\overline{A} \tag{5}$$

where $\overline{A}$ is the average A in the interval (τ_0, τ^*). The baroclinic process acting for 1000 s can produce enough circulation to account for a strong tornado with circulation of 5×10^4 m^2 s^{-1} and a damage path 400 m wide (based on a outer potential vortex and a damaging-wind threshold of 40 m s^{-1}) if $\overline{A} =$ 50 m^2 s^{-2}. This value is feasible because $\overline{A}$ was about 100 m^2 s^{-2} in Rotunno and Klemp's (1985) simulation (albeit with the microphysical problems listed above). Now suppose that the boundary of $\overline{A}$ in (b, z) space is an ellipse with axes of

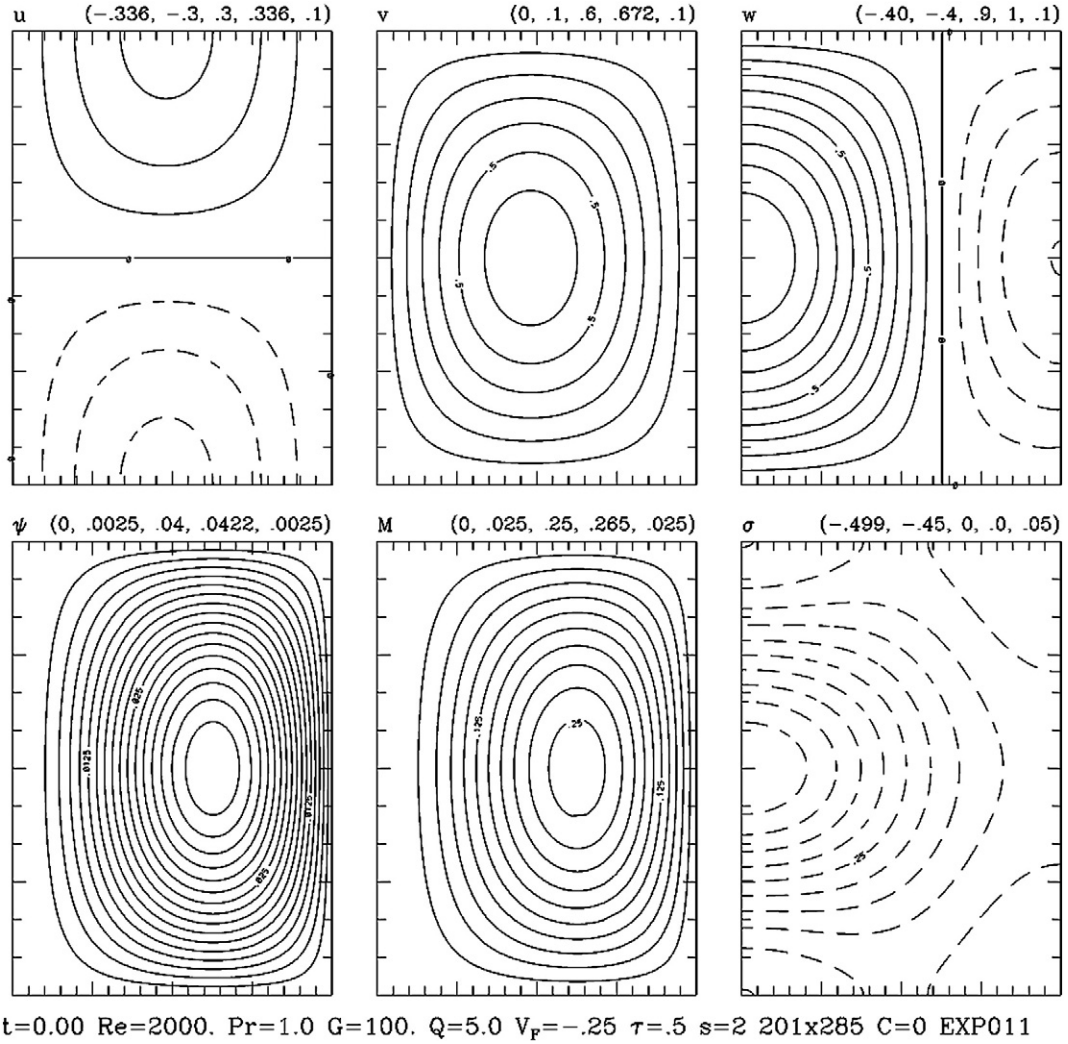

Fig. 5. Initial fields in a tornadogenesis model. The fields, in a radial-height (r-z) cross-section with the axis $r = 0$ on the left side, are (clockwise from top left) radial, tangential and vertical wind, pressure, angular momentum and streamfunction. The domain is 1 unit tall, 0.7 units in radius, and the thermodynamic speed limit (maximum initial vertical wind) is 1. The key to the list in the parentheses is (minimum value, minimum contour value, maximum contour value, maximum value, contour interval). To roughly scale up to a real supercell, multiply lengths by 12,000 m, velocities by 34 m s^{-1}, pressures by 1156 pa, angular momentum by 4.1×10^5 m^2 s^{-1}, and streamfunction (volume flow rate/2π) by 4.9×10^9 m^3 s^{-1}. From Davies-Jones (2008).

lengths $z_2 - z_1$ and $b_2 - b_1$ (where $z_2 - z_1$ is the circuit's height span and $b_2 - b_1$ is the maximum horizontal buoyancy difference across the circuit). Then

$$\overline{A} = \frac{\pi}{4}(z_2 - z_1)(b_2 - b_1) \tag{6}$$

For $\overline{A} = 50\ \mathrm{m^2\ s^{-2}}$ and $z_2 - z_1 = 1000$ m, $b_2 - b_1 = 0.064\ \mathrm{m\ s^{-2}}$, which corresponds to a maximum horizontal temperature difference $\Delta T = (b_2 - b_1)T/g$ of just 2 K for $T = 300$ K. This small temperature difference should not change much as the material circuit flattens out from low altitudes and contracts. In principle, a thermal difference is not required at all. The buoyancy difference can be composed entirely of a difference in precipitation loading of 6 g $\mathrm{kg^{-1}}$ $[=(b_2 - b_1)/g]$.

3.3. Barotropic mechanism: Fujita's 'recycling process'

Ideally, tornadoes can form barotropically as a result of some high-angular-momentum air being transported downward and inward towards the axis of rotation. Fujita (1975) proposed this mechanism, which he called the recycling process, after observing in an eyewitness film that the rotating rain streaks fell towards a tornado.

Davies-Jones (2008) simulated this process using a simple axisymmetric model without buoyancy forces. This model has some nice features. The domain is closed with a complete storm-scale circulation so that there can be a realistic two-way interaction between a tornado and its parent storm. The domain is nonrotating to reflect the insignificance of the Earth's vorticity in supercell environments (Davies-Jones, 1984). The boundary conditions are impermeable walls with no slip on the tangential wind, free slip (no stress) on the

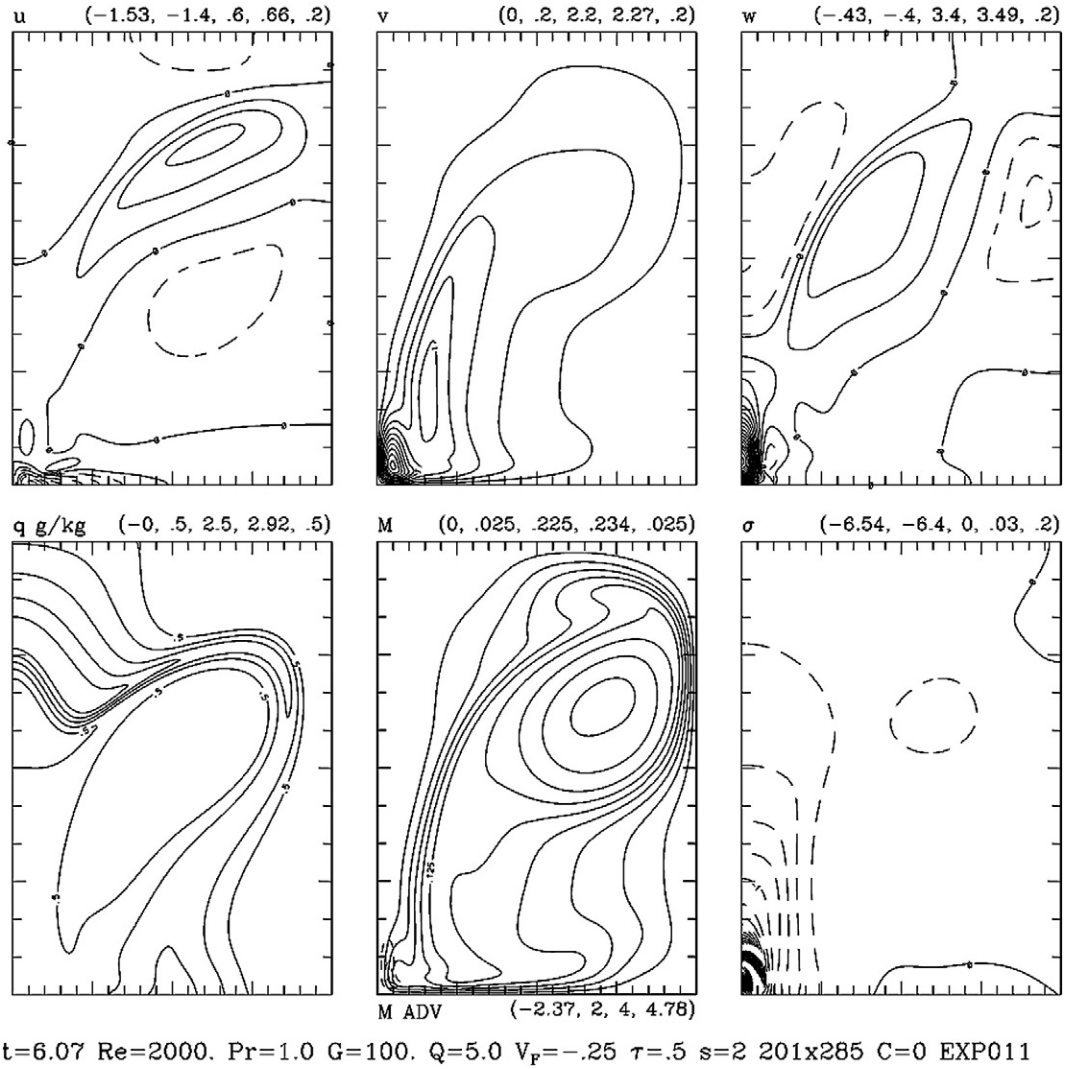

Fig. 6. Fields at time of maximum tornado intensity in the tornadogenesis model. The time, when scaled up, is 36 min. The precipitation mixing ratio in g/kg is shown here instead of the streamfunction and two contours (dashed, contour values 2 and 4) of angular-momentum advection are included in lower center panel. From Davies-Jones (2008).

other wall-parallel wind component. These boundary conditions are the ones satisfied by the initial Beltrami flow, and are the best ones to use at the ground (i.e., $du/dz = v = w = 0$ at $z = 0$) in an axisymmetric model with constant eddy viscosity because the radial velocity in the turbulent boundary layer of a strong vortex peaks just off the surface at the bottom of the layer (Lewellen, 1993, p. 24). The side of the domain does not rotate so angular momentum is not imparted to the flow artificially. The initial condition is a Beltrami flow (vorticity parallel to velocity everywhere) that resembles a mid-altitude mesocyclone with a cyclonic updraft surrounded by an anticyclonic downdraft (Fig. 5). Air near the ground has little angular momentum initially. Winds in the corner region (where the surface-based inflow turns upward into the vortex) are light initially. The initial flow is balanced (apart from a slow viscous decay). In other words, if it is left unperturbed, its pattern does not change and a vortex does not form as an unintended consequence of either an unbalanced initial state or boundary conditions that create imbalances.

To simulate tornadogenesis, hydrometeors in moderate amount are introduced through the top into the divergent flow above the mature updraft; they fall around the side of the updraft in a realistic rain curtain (albeit axisymmetric) on the scale of a radar hook (roughly 5 km in radius, Markowski, 2002b) and drag air with substantial angular momentum downward. The rotating updraft narrows as it is squeezed by the precipitation-induced downdraft. The squeezing and downward transport of air with fairly high angular momentum causes the mesocyclone to contract, descend, and spin up a bit. The mesocyclone comes within about 10% of being in cyclostrophic balance as its diameter steadily decreases to less than 3 km and its maximum in tangential velocity steadily moves downward to around 2 km. As the air in the enhanced downdraft hits the ground, some of it flows inwards towards the nadir of the axis. A new maximum of tangential velocity forms near the ground and moves inwards. The near-ground vortex becomes more intense than the one above, and then rapidly intensifies into a tornado, which is capped by the wider vortex aloft (Fig. 6).

In this simulation, the axisymmetric rotating rain curtain instigates the tornado by dragging down air with moderate angular momentum down to the ground. The mechanism is unequivocally barotropic because differential drag forces generate azimuthal vorticity, which cannot be tilted into the vertical in an axisymmetric flow. From the perspective of Lewellen and Lewellen (2007), the precipitation-induced downdraft causes the corner flow of the mesocyclone to collapse to smaller radii by blocking the no-swirl surface inflow of the original Beltrami flow and bringing air with angular momentum down into the inflow where it spins up as it approaches the axis. Collapse causes dramatic increases in peak velocities and pressure deficits with concomitant drops in their locations to near the ground. Corner flow collapse (Lewellen et al., 2000) and downward transport of vertical vorticity to the ground where there is none previously (Davies-Jones, 1982a,b) are two sides of the same coin.

Remarkably, a simple axisymmetric model without buoyancy, environmental stratification and release of latent heat, can simulate several observed features of tornadogenesis even though axisymmetry requires the mechanism to be barotropic. The model reproduces on the mesocyclone scale an anticyclonic clear-slot intrusion of descending air, a collapsing top, and contraction and lowering of the mesocyclone prior to the tornado. The most intense winds in the mesocyclone reach the thermodynamic speed limit (Snow and Pauley, 1984; Fiedler and Rotunno, 1986). On the small scale, it generates a tornado with an axial jet capped by a vortex breakdown that is an abrupt transition to the constricted mesocyclone aloft. Its winds easily exceed the thermodynamic speed limit. At low levels, practically all the rising air is contained in the tornado itself. Tornadogenesis still occurs in a 3D version of the model (Kis et al., 2008) that doesn't have axisymmetry constraints, such as the one that makes the inward part of the outflow converge towards a focal point (the imposed axis).

Fully 3D numerical cloud models are of course far more accurate because they include tilting of baroclinically generated vorticity and more realistic thermodynamics, microphysics and turbulence effects, but diagnosing how tornadoes form in them is very difficult (Rotunno, 1986). Tornadogenesis in the axisymmetric model is much easier to interpret. For example, the vortex lines lie in the surfaces of constant angular momentum (M), which are closed because the domain is nonrotating and because a no-slip condition is imposed on the tangential wind at the boundaries. The directed vortex lines that enter the tornado emanate from the triggering downdraft where they are downward, indicative of anticyclonic vorticity there. From the base of the downdraft the lines stretch radially inward until they reach the tornado where they turn abruptly upward into the core.

3.4. Circulation around a horizontal curve

Instead of computing barotropic and baroclinic circulation around a material curve, we can compute circulation around a horizontal closed curve that is stationary relative to the storm. The rate of change of absolute circulation Γ_a around a horizontal curve L that is moving with a storm (at velocity $\mathbf{c}$) is

$$\frac{\delta\Gamma_a}{\delta t} = -\oint_L (\zeta + f)(\mathbf{v}_H - \mathbf{c}) \cdot \mathbf{n} ds - \oint_L w\left(\frac{\partial \mathbf{v}_H}{\partial z} + 2\boldsymbol{\Omega}\right) \cdot d\mathbf{x} + \oint_L p d\alpha + \oint_L \mathbf{F} \cdot d\mathbf{x} \tag{7}$$

where $\mathbf{v}_H$ is the horizontal wind, $\boldsymbol{\Omega}$ is the Earth's angular velocity, $d\mathbf{x} = (dx, dy, 0)$, $\mathbf{n}$ is the outward horizontal unit normal to L, ds is an element of arclength, $\mathbf{n}ds = (dy, -dx, 0)$, and α is specific volume (Davies-Jones, 2004). Eq. (7) is the areal integral of the vertical-vorticity equation with the terms on the right being (after use of Stokes' theorem) the areal integrals of the horizontal advection of the absolute vertical vorticity $\zeta + f$, vertical advection of ζ, the solenoidal term, and the frictional torque, respectively. The horizontal component of $\boldsymbol{\Omega}$ appears in the second term on the right. Since it is smaller compared to $|\partial \mathbf{v}_H/\partial z|$, we neglect it henceforth. When L is a circle C of radius r_0, Eq. (7) becomes

$$\frac{\delta\Gamma_a}{\delta t} = -\oint_C U \frac{\partial M_a}{\partial r} d\phi - \oint_C w \frac{\partial M_a}{\partial z} d\phi + \oint_C p d\alpha + \oint_C r_0 F_\phi d\phi \tag{8}$$

where (U, V, w) is the storm-relative wind in cylindrical coordinates (r, ϕ, z) coaxial with C, M_a is the absolute angular

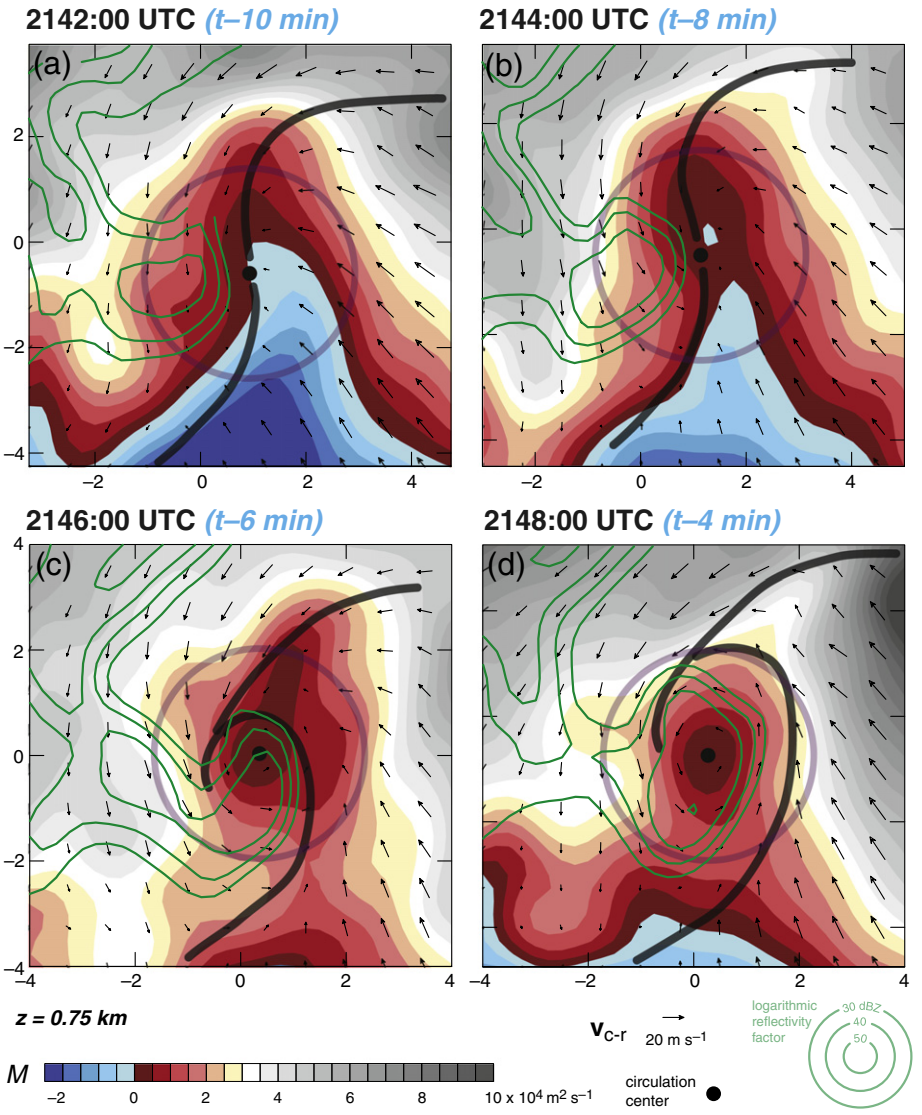

Fig. 7. Analyzed fields in the Goshen County, Wyoming tornado storm of 5 June 2009. The fields are at 750 m above the ground and at (a) 10, (b) 8, (c) 6 and (d) 4 min prior to tornado touchdown. The data were collected during the VORTEX2 field experiment. The color-shaded contours are for angular momentum M relative to the circulation center (black dot). The green contours are for DOW7 logarithmic reflectivity (contours start at 30 dBZ and the contour interval is 10 dBZ). The vectors are horizontal winds in the reference frame of the moving circulation center. Gust fronts are indicated with heavy gray lines. Axis labels are in km. A 2-km-radius circle around the circulation center is overlaid in each panel. From Markowski et al. (2012).

momentum $Vr + fr^2/2$ about the center of C, and F_ϕ is the tangential component of the friction force. In this special case, circulation changes through radial and vertical advection of angular momentum (AM) on the circle, solenoids (Dutton, 1986, p. 373) and frictional torque.

Markowski et al. (2012) showed relative angular momentum $M \equiv Vr$ with respect to the circulation axis in an observed tornadic storm (Fig. 7). They did not include the Earth's angular momentum because it is insignificant [less than 2×10^3 m^2 s^{-1} for $r < 6$ km]. In their paper C is a circle of 2 km radius around the circulation center. At 10 min prior to tornado touchdown (Fig. 7a), the circulation center is on the boundary between the storm's warm inflow and cool outflow. Air from the warm sector is heading almost directly towards the circulation center and radial advection of AM is either weakly positive or negative. In the warm-sector $-w\partial M/\partial z$ is negative because air with lower AM is rising (Fig. 8a). This is detrimental to low-level rotation. Thus there is little contribution to circulation gain around C from advection of AM on the side of the circle that is in the warm sector. In contrast, air from behind the gust front (GF) enters the circulation obliquely and there is considerable horizontal advection of AM. Moreover, the vertical advection of AM is less negative behind the GF than in the warm sector and it is positive on the northwest arc of C.

Four minutes prior to the tornado, the situation looks far more favorable for tornadogenesis. The rear-flank gust front (Markowski, 2002b) has advanced around the circulation and

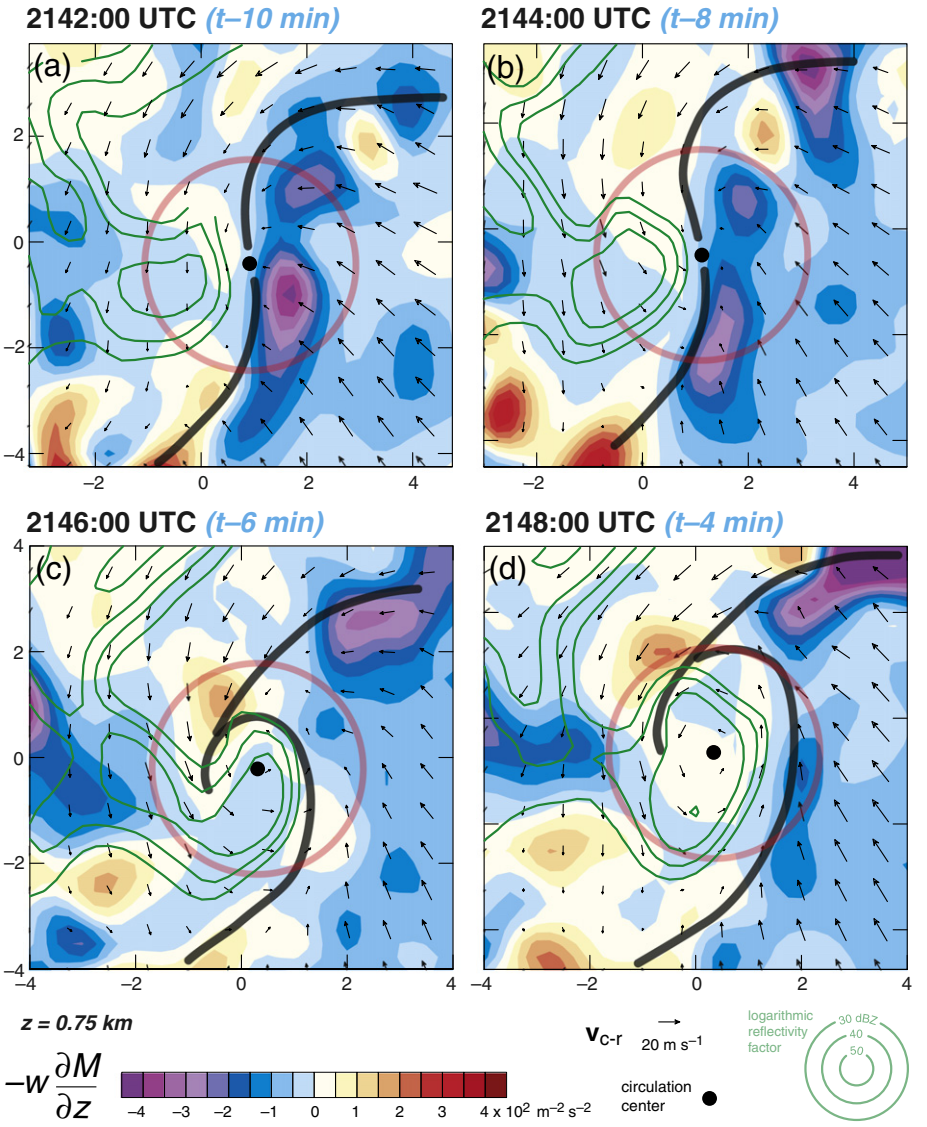

Fig. 8. As in Fig. 7, but for vertical advection of angular momentum, $-w\partial M/\partial z$, instead of angular momentum M (unpublished, courtesy of P. Markowski).

the low-level cyclone has occluded with the circulation center now in the cool air (Fig. 7d). The warm-sector air with low AM has been blocked off from the circulation and air with higher AM has subsided in the rear-flank downdraft and wrapped around the center (Fig. 8d). The rotation has intensified because the rear-flank downdraft has collapsed the corner flow of the cyclone.

4. Stage 3 of tornadogenesis: tornado formation or failure

We have got ahead of ourselves in Section 3.3 by not stopping the discussion at the end of stage 2, when rotation first develops at ground level as a result of the rear-flank downdraft transporting vertical vorticity down to the ground. The low-level vortex is beneath a mesocyclone aloft that has lowered, narrowed and intensified.

4.1. Tornado formation

In convergent flow beneath a strong updraft, the low-level vortex contracts horizontally and spins up. This hypothesis is consistent with analyses that reveal strong low-altitude convergence prior to the tornado and a large vertical stretching term with a maximum at the tornado. In simulations without surface friction, centrifugal forces increase during the contraction until they come into cyclostrophic balance with the inward pressure-gradient force. The vortex then stops contracting. Because of the free-slip (no-stress) condition at the ground, the balance extends all the way to the surface. Therefore, winds cannot exceed a thermodynamic speed limit (Section 6) based on cyclostrophic and hydrostatic theory. At worst, there is a weak, broad tornado.

The scenario changes radically when surface friction is included in the model. In most circumstances friction moderates

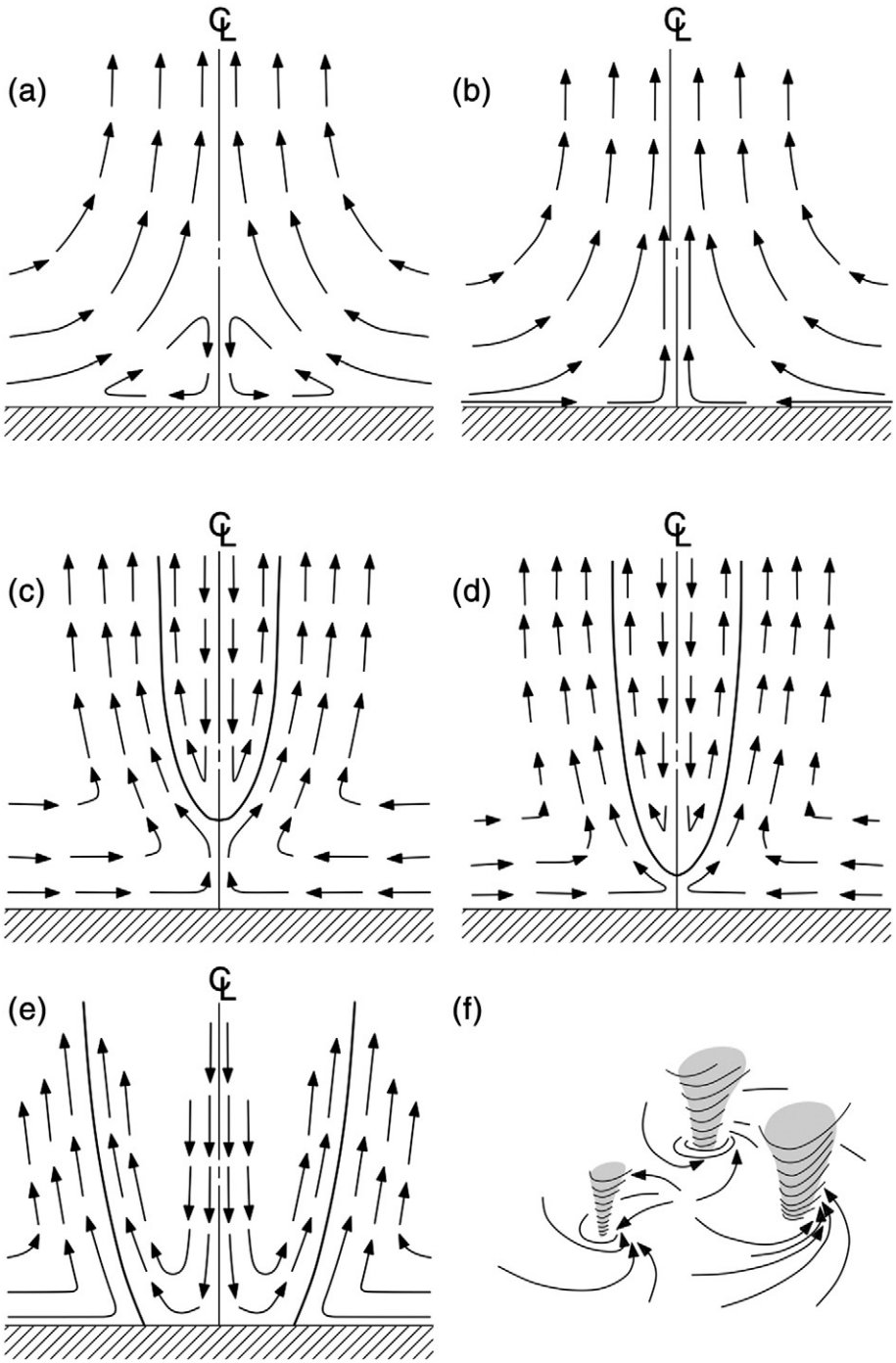

Fig. 9. Effect of increasing domain swirl ratio on tornado flow structure. From Davies-Jones et al. (2001).

the winds. Paradoxically, surface friction greatly intensifies the vortex by upsetting cyclostrophic balance in a thin boundary layer. The way this happens is explained in Section 6.

4.2. Tornadogenesis failure

Doppler-radar analyses reveal storms in which tornadoes seem imminent within minutes, but don't happen. Several factors can disrupt tornadogenesis. For instance, the storm-relative convergent inflow may be too weak to prevent cold-air outflow from surging ahead of the updraft. The updraft loses its roots as a deep layer of dense stable air intrudes beneath the updraft. Using models with idealized thermodynamics, buoyancy forces, and precipitation, Markowski et al. (2003) and Markowski and Richardson (in press) showed that a tornado would not form if the air at the ground were so

dense and stable that the overlying rotating updraft cannot pull it upwards.

Ward's (1972) laboratory model illustrates other failure modes. A tornado will not form at the circulation center if the updraft has insufficient rotation because the boundary layer separates before air reaches the axis (Fig. 9a). Also a tornado will not form on the axis of rotation if the updraft's rotation is too strong. In this situation, strong centrifugal forces establish cyclostrophic balance at large radii and prevent the convergence of air to near the axis, resulting in a broad weak central vortex. However, multiple tornadoes may still form around the periphery of the large vortex (Fig. 9f).

5. Tornado structure

Before starting the detailed explanation of how tornadoes form, we detail the different types of tornadoes for subsequent reference. In Ward's (1972) laboratory vortex chamber, which is the one with the most dynamical and geometric similarity to tornado environments, the range of vortices is similar to the observed spectrum of tornadoes. The type of miniature tornado is controlled largely by the domain swirl ratio, S, which is the ratio of the tangential velocity at the updraft edge divided by the mean updraft velocity. As the swirl ratio increases, vortex structure changes as illustrated in Fig. 9 and summarized in more detail by Davies-Jones et al. (2001). At very low swirl (Fig. 9a), there is no tornado. Flow in the boundary layer separates and passes around the corner flow. At low S (Fig. 9b) there is a smooth-flowing, one-cell, weak tornado with upward flow along the axis. At moderate S (Fig. 9c), the end-wall boundary layer erupts upward into an extremely strong, smooth, spiraling, vertical jet (an end-wall jet). The flow in the end-wall jet is supercritical, which means that, unlike subcritical flow, centrifugal waves (and information) cannot propagate against the flow (i.e., downwards) because the air is moving upwards more rapidly than the fastest downward propagating wave. The jet inevitably slows down as it encounters slower air aloft, and at the height where the upward air velocity is critical (i.e., equal to the fastest downward wave speed) the vortex breaks down into a conjugate subcritical vortex aloft with the same circulation at radial infinity as the end-wall vortex. Mass and axial-momentum fluxes are conserved through the transition, but energy is lost (Fiedler and Rotunno, 1986). The conjugate vortex is a two-cell vortex with downdraft on the axis surrounded by updraft. It is much broader and weaker, turbulent, and subcritical. [The circular hydraulic jump visible in a kitchen sink when the water is flowing is similar to vortex breakdown, except the waves are external gravity ones with a vertical restoring force instead of centrifugal ones with a radial restoring force (Markowski and Richardson, 2010, p. 49). Water from the tap spreads along the surface initially in a shallow outflow at supercritical speed, slows in the diverging flow to conserve mass, enters the hydraulic jump as its speed becomes critical, and thereafter moves at subcritical speed in a much deeper conjugate outflow.] At slightly higher S (Fig. 9d), the breakdown stagnation point descends very close to the ground and the end-wall vortex is confined to the boundary layer. This structure is called a drowned vortex jump. At still higher S (Fig. 9e), the central downdraft extends to the ground and there is a turbulent two-cell vortex with the inflow now erupting upward in an annular corner region. With further increases in S the core radius increases rapidly and the flow resembles a cylindrical sheet of high vorticity. At large S the vortex sheet becomes unstable (Rotunno, 1978) and the large vortex morphs into two secondary vortices, which orbit rapidly around the central axis of the system. With increasing S (Fig. 9f), the flow chaotically transitions from two to three revolving secondary vortices, then to four, five and six.

The domain swirl ratio only incorporates the constant angular momentum of the inflow air above the boundary layer in Ward's apparatus. Lewellen et al. (2000) devised another parameter, the corner swirl ratio, which takes into account the existence of lower angular momentum in the boundary layer. Two flows with the same domain swirl ratio can have quite different corner swirl ratios owing, for example, to diverse surface roughness. Consequently, these flows can have dissimilar structures in the corner flow region and considerably different maximum wind speeds.

The tornadoes with the highest wind speeds are probably those with end-wall vortices, and large two-celled vortices with (and perhaps sometimes without) secondary vortices. The secondary vortices are particularly dangerous because they move rapidly around the axis of the parent vortex and because they may be supercritical near the ground.

A typical tornado dies by 'roping out'. Subsiding cold air with low angular momentum overtakes the tornado near the ground (Rasmussen and Straka, 2007). The top and bottom of the visible tornado then follow divergent paths. The vortex becomes greatly tilted and stretched into a rope shape. Waves are seen traveling down the funnel. The visible funnel becomes serpentine and may even break into segments before it disappears from view. Vortex instability seems to be the cause of death.

Damage surveys and Doppler-radar observations suggest that a few tornadoes decay by broadening and weakening. Demise of these tornadoes is consistent with decline of the overlying parent updraft. If the upward buoyancy and inertial forces aloft become weaker than downward pressure-gradient forces (associated with precipitation drag and/or the mesocyclone spreading with height), the net downward force would drive a downdraft that envelops the tornado and fills it from above. In the diverging flow, the tornado would widen and spin down as observed. This process (sans buoyancy) ends the tornado in the Davies-Jones (2008) axisymmetric model.

6. Tornado dynamics

Three important topics in tornado dynamics are the source of rotation (already covered in Section 4), the energy source (Section 6.1), and the mechanism that makes them far more powerful that expected on the basis of simple theory (Section 6.2).

6.1. No need for exotic energy sources

In the past, scientists have proposed extraordinary sources of energy to explain the awesome power of tornadoes. One postulate was that heating from repeated lightning strikes down the same channel causes tornadoes. Early during the Tornado Intercept Project, it became evident that tornadoes

generally develop from precipitation-free, updraft cloud bases with the nearest cloud-to-ground lightning and precipitation a few kilometers away (Davies-Jones and Golden, 1975). Thus, the above theory was discounted, as were ones that relied on precipitation falling along the axis of the developing tornado or placed the formative tornado in a downdraft rather than an updraft.

Meteorologists (e.g., Davies-Jones and Kessler, 1974) used to place an upper limit (now called the 'thermodynamic speed limit') on tornado wind speeds based on assumptions of hydrostatic and cyclostrophic flow. Before describing the method, we note that, with use of the equation of state for air ($p\alpha = RT$), the pressure-gradient force (PGF), $-\alpha\nabla p$, can be written as $-c_p\theta\nabla\pi$ where R is the gas constant for air, c_p is the specific heat of air at constant pressure, $\theta \equiv T/\pi$ is the potential temperature, T is temperature, $\pi \equiv (p/p_0)^{R/c_p}$ is a non-dimensional pressure, and p_0 is a reference pressure (1000 mb). For steady axisymmetric flow in cylindrical coordinates, the equation of vertical motion is

$$\frac{d}{dz}\left[\frac{w^2(0,z)}{2}\right] = -c_p\theta(0,z)\frac{d\pi(0,z)}{dz} - g + \mathbf{k}\cdot\mathbf{F}(0,z) \tag{9}$$

on the axis and

$$0 = -c_p\theta(\infty,z)\frac{d\pi(\infty,z)}{dz} - g \tag{10}$$

in the far environment (at $r = \infty$) where the pressure is hydrostatic. By subtracting Eq. (10) from Eq. (9), approximating θ by a mean value $\bar{\theta}$ in the PGF term, and then integrating from the top of the boundary layer at $z = \delta$ to the level of neutral buoyancy (LNB) at $z = H$ near the tropopause, we obtain

$$\frac{w^2(0,H)}{2} - \frac{w^2(0,\delta)}{2} \approx c_p\bar{\theta}\Delta\pi(\delta) - c_p\bar{\theta}\Delta\pi(H) + \mathrm{CAPE} + D \tag{11}$$

where $\Delta\pi(z) = \pi(0, z) - \pi(\infty, z)$, and CAPE and D are the line integrals along the axis from $z = \delta$ to $z = H$ of the buoyancy and friction forces, respectively. For estimating updraft speeds by the parcel method, only the firstterm on the left and CAPE are retained. We thus obtain

$$w(0,H) = (2\ \mathrm{CAPE})^{1/2}. \tag{12}$$

The maximum vertical velocity is at the LNB and the updraft overshoots into a cool top in the stratosphere. The resulting outward hydrostatic PGF drives outflow into the storm anvil. A rotating updraft does not have to overshoot the LNB because the centrifugal force can accelerate the upper-level outflow (Lilly, 1969). If this is the case, then $w(0, H) = \Delta\pi(0, H) = 0$ and (11) becomes

$$-c_p\bar{\theta}\Delta\pi(\delta) \approx \frac{w^2(0,\delta)}{2} + \mathrm{CAPE} + D. \tag{13}$$

We specify a cyclostrophic balance of radial forces to prevent air from rushing inward to fill the partial vacuum. Integrating the cyclostrophic equation for a specified vortex flow $V(r)$ gives us

$$-c_p\bar{\theta}\Delta\pi(\delta) = \int_0^\infty \frac{V^2(r)}{r}dr = \beta V_m^2 \tag{14}$$

where V_m is the maximum tangential wind, and $\beta = 0.5$ for a vortex with a stagnant core and outer potential vortex (where $V \propto 1/r$) and $\beta = 1$ for a Rankine combined vortex, which has a core in rigid rotation and an outer potential vortex. From Eqs. (13) and (14)

$$V_m = \left[\frac{0.5w^2(0,\delta) + \mathrm{CAPE}}{\beta}\right]^{0.5} \tag{15}$$

if D is negligible. The thermodynamic speed limit is obtained by neglecting $w(0, \delta)$ as well. Then the surface pressure deficit of the tornado is hydrostatic and equals the weight deficit of the warm core. The vortex with the stagnant core yields the highest speed limit. In this case the kinetic-energy limit equals the CAPE of the environment. The thermodynamic speed limit works well for tornadoes in simulations without surface friction because $w(0, \delta)$ is then negligible.

Note that buoyancy and CAPE are estimated traditionally based on a parcel ascending pseudoadiabatically once it becomes saturated. For a two-celled tornado with a central downdraft, adiabatic warming of parcels in descent makes the hydrostatic pressure deficit much larger, resulting in a considerably higher speed limit than the traditional one (Lilly, 1969). When assessing whether wind speeds measured in a tornado exceed the thermodynamic speed limit, the scientist also must remember to add the tornado's translation speed to the limit. Tornadoes cross the land at speeds from 0 to above 25 m s^{-1}.

Lewellen (1976), Snow and Pauley (1984), and Fiedler and Rotunno (1986) realized that the thermodynamic speed limit and the associated kinetic-energy limit could be broken by purely fluid-dynamical effects. There is no need for exotic energy sources because there is a process, described in Section 6.2, which enables the pressure-gradient force to do extra work on a parcel, thereby increasing the parcel's kinetic energy beyond the limit.

6.2. Paradoxical role of friction

The Davies-Jones (2008) model produces a near-ground cyclone both with and without surface friction during stage 2 of tornadogenesis. Stage 3, the contraction of this cyclone into a tornado, happens only in simulations with surface friction. A frictional torque between the cyclone and the ground is essential to tornado formation because it induces strong radial inflow along the ground as follows. Parcels in the boundary layer of the tornado lose angular momentum to the ground owing to the torque. The cyclostrophic balance of forces in the radial direction that exists without surface friction is upset in the boundary layer, where the inward pressure-gradient force is greater than the reduced outward centrifugal force and drives strong radial inflow. Consequently, parcels penetrate much closer to the axis than the equilibrium radius of cyclostrophic balance above the

boundary layer. Because their angular-momentum loss to the ground is fairly small, they revolve very quickly near the axis (like an ice skater going into a spin). To conserve mass, the radial inflow in the boundary layer has to turn the corner as it approaches the axis. It erupts violently upward in a high-speed axial jet and a supercritical end-wall vortex forms in the corner region. The axial swirling jet may be thought of as an upward continuation of the boundary layer. A new cyclostrophic balance supports the very low pressure on the axis arising from the Bernoulli effect of the vertical jet. The thermodynamic speed limit is violated for the following reason. Inviscid theory neglects the turbulent boundary layer and thus can be applied only from the top of the boundary layer, say $z = \delta$, not from the ground upwards. Overall hydrostatic balance between $z = \delta$ and the tropopause becomes a bad approximation because $w(0, \delta)$ is far from zero.

To find out how kinetic energy exceeds its limit in the end-wall vortex, we look at the mechanical-energy equation, which is

$$\frac{d}{dt}\left(\frac{U^2+V^2+w^2}{2}+gz\right) = -c_p\theta\mathbf{v}\cdot\nabla\pi+\mathbf{v}\cdot\mathbf{F} \tag{16}$$

where U, V and w are the radial, tangential and vertical components of the wind $\mathbf{v}$. For a parcel of unit mass, the rate of change of its kinetic energy plus its potential energy (PE) is equal to the work rate of the PGF plus the work rate of the friction force $\mathbf{F}$. The parcel gains PE as it rises in the vertical jet so it cannot gain KE from its PE. In a boundary layer friction acts to reduce KE. Therefore, the parcel can only acquire KE in excess of CAPE if the PGF does more work. In the unreal case where there is no surface stress, the speed limit is not broken because the centrifugal force balances the radial PGF all the way to the ground. The centrifugal force does no work but transfers radial kinetic energy $U^2/2$ to tangential kinetic energy $V^2/2$ when flow is inward. By decelerating the inflow, it inhibits the work done by the radial PGF. With surface stress, the centrifugal force is reduced in the boundary layer, enabling the PGF to do far more work there in this case. Only through this extra work by the PGF can we account for KE far in excess of CAPE.

For flow that is steady, inviscid, and adiabatic or pseudoadiabatic, there is a Bernoulli (energy-conservation) principle, which is derived using both the mechanical energy equation and a thermodynamic energy equation. For steady flow,

$$-c_p\theta\mathbf{v}\cdot\nabla\pi = -c_p\theta\frac{d\pi}{dt} \tag{17}$$

so positive work done by the PGF is associated with a loss of parcel pressure. We use the identity

$$-c_p\theta\frac{d\pi}{dt} \equiv T\frac{dS}{dt}-\frac{d\left(c_pT\right)}{dt} \tag{18}$$

where $S \equiv c_p \ln\theta$ is the specific dry entropy and c_pT is the specific dry enthalpy. For a parcel undergoing adiabatic and then pseudoadiabatic expansion, the thermodynamic energy equation (or first law of thermodynamics) is

$$T\frac{dS}{dt} = -L\frac{dq}{dt} \tag{19}$$

where L is the latent heat of condensation and q is the vapor mixing ratio (conserved until the parcel becomes saturated). By disregarding the small variation of L with T, we find from Eqs. (18) and (19) that

$$c_p\theta\frac{d\pi}{dt}\approx\frac{d\left(c_pT+Lq\right)}{dt}=\frac{dk}{dt} \tag{20}$$

where Lq is the specific latent energy and $c_pT + Lq \equiv k$ is approximately the specific moist enthalpy. By Eqs. (17) and (20) the work done by the PGF equates to the enthalpy lost by the parcel. For steady adiabatic and pseudoadiabatic flow with negligible friction, Eqs. (16), (17) and (20) give us the conservation law

$$\frac{U^2+V^2+w^2}{2}+gz+k = \text{constant}, \tag{21}$$

i.e., the total energy of a parcel, the sum of its specific KE, PE and moist enthalpy, is conserved. In this case, a parcel has to lose additional moist enthalpy in order to gain KE in excess of the limit. From Eq. (20) this enthalpy loss must stem from a further lowering of pressure.

As an example, consider a parcel initially at 1000 mb with a temperature of 26 °C, a dewpoint temperature of 20 °C, and a mixing ratio of 14.9 g kg^{-1}. After adiabatic expansion to its condensation pressure of 915 mb and then pseudoadiabatic expansion to 800 mb, this parcel has a temperature of 13.6 °C, a mixing ratio of 12.3 g kg^{-1}, and a moist enthalpy loss of 18,800 J kg^{-1}. At 800 mb in a normal thunderstorm updraft, the vertical velocity is perhaps 14 m s^{-1}, and the enthalpy loss is balanced almost entirely by a gain in PE associated with a parcel vertical displacement of 1900 m. Only 0.5% of the enthalpy loss is converted into KE gain. At 800 mb in a vertical jet, the vertical displacement may be only 100 m, and, from Eq. (21), the upward speed is then 189 m s^{-1}. In this case the KE obtains 95% of the enthalpy loss and the PE only 5%. The upward speed is far in excess of the thermodynamic speed limit, which based on a stagnant-core vortex and a typical CAPE of 2500 J kg^{-1} in tornado environments is around 70 m s^{-1}.

Thus, surface friction paradoxically instigates the extreme pressure deficits and upward and rotary winds in end-wall tornadoes. It can cause maximum winds in quasi-steady tornadoes to increase to 3–4 times the speed limit in the vertical component, more than twice it in the tangential velocity, and 1.5 times it in the radial inflow, and maximum pressure deficits to magnify to about nine times the hydrostatic-deficit value. Remarkably, vortex dynamics can cause the maximum vertical velocity in the storm to be very close to the ground instead of near the tropopause. Extremely high vertical kinetic energy, $w^2/2$, in the axial jet is balanced in Bernoulli's equation by the extreme pressure drop, which in turn is supported by cyclostrophic balance that prevents air from flowing inward to fill the void. Lewellen and Lewellen (2007) showed that

even larger quasi-steady amplifications could happen if the inflow satisfies some unlikely specific conditions, and still larger transient ones could arise with certain collapses of the corner region triggered by instantaneously blocking part of the surface-based inflow at the side boundary.

7. Summary

The genesis of tornadoes in supercells divides naturally into three stages. Initial development of a mesocyclone aloft (stage 1) is a consequence of a barotropic process, tilting by the updraft of streamwise vorticity present in the storm-relative inflow. The preponderance of the evidence points to the development of near-ground rotation in dense subsiding outflow air (stage 2) being a baroclinic process. Stage 2 is initiated by the rear-flank gust front blocking inflow air with low angular momentum and bringing down air with higher angular momentum from aloft. There is now air in rotation at ground level. In stage 3, this air flows inward along the ground towards the circulation center and its rotation increases. Without surface friction, increasingly strong centrifugal forces balance the inward pressure-gradient force, thus stopping the convergence of parcels and preventing tornado formation. With frictional stress at the ground, cyclostrophic imbalance in the vortex boundary layer causes the air to overshoot its cyclostrophic equilibrium radius (the one associated with the cyclostrophic balance needed to maintain the hydrostatic-pressure deficit of the vortex core). The boundary layer erupts violently upwards near the axis in a spiral jet with tornadic winds greatly in excess of those predicted on the basis of hydrostatic and cyclostrophic balance. A different cyclostrophic balance is established to support the extremely low central pressure arising from the Bernoulli effect of the vertical jet.

Acknowledgments

I thank the Scientific Programme Committee for inviting me to give a keynote address at the 7th European Conference on Severe Storms and the Finnish Meteorological Institute for funding my participation in the conference. Dr. Jerry Straka provided a very helpful review of the first draft. I am also grateful for insightful comments provided by Dr. Paul Markowski and an anonymous reviewer.

Appendix

Here we derive a formula for the time that an updraft of finite radius takes to concentrate Earth's vorticity into a strong vortex. Consider inviscid axisymmetric flow at a flat ground ($z = 0$). At an initial time $t = 0$, a radial inflow along the ground

$$u(r,t) \equiv \frac{dr}{dt} = \begin{cases} -Cr/2 & \text{if } r \le r_u \\ -Cr_u^2/2r & \text{if } r \ge r_u \end{cases} \tag{A1}$$

starts impulsively and continues indefinitely. The radial flow consists of an inner convergence zone (CZ) of radius r_u and area a_u beneath an updraft, surrounded by non-divergent confluent flow outside the CZ. In Eq. (A1) C is the constant horizontal convergence in the CZ. Initially, the absolute vertical vorticity $\zeta + f$ equals f to isolate the planetary vorticity as the origin of subsequent rotation. Let $R(0)$ and $A(0)$ be the initial radius and area of a fluid circle that has radius $R(t)$ and area $A(t)$ at time t. In the absence of torques the absolute circulation of the fluid circle, Γ_a, is conserved. Therefore,

$$\Gamma_a = fA(0) = [f + \zeta(t)]A(t). \tag{A2}$$

The applicable vertical-vorticity equation is $d\ln(f + \zeta)/dt = C$ inside the CZ and $= 0$ outside the CZ. Thus, the absolute vertical vorticity on a fluid circle initially outside the CZ does not increase for the time t_{out} that it takes to reach the edge of the CZ and thereafter increases exponentially. The fluid parcels that comprise the CZ initially form an inner kernel that spins up rapidly as its area contracts. The kernel radius is given by $r_k(t) = r_u \exp(-Ct/2)$. These parcels all endure identical vertical stretching and so the vorticity in the kernel is spatially uniform. Hence, the absolute vertical vorticity of a fluid circle is given by

$$f + \zeta(t) = \begin{cases} f & \text{for } R(t) \ge r_u \\ f\exp[C(t - t_{out})] & \text{for } R(0) \ge r_u \ge R(t) \\ f\exp(Ct) & \text{for } r_u \ge R(0) \end{cases}. \tag{A3}$$

The absolute circulation of the kernel is $f\pi r_u^2$, which is only 5×10^3 m^2 s^{-1} even for a large CZ of radius 4000 m. This is smaller than the circulation of almost all tornadoes (Davies-Jones and Kessler, 1974, p. 564). Therefore, we assume that the air parcels that form the tornado originate in the confluent region and are stretched tremendously in the CZ. Thus, the fluid circles of interest are those for which $R(0) \ge r_u \ge R(t)$. By integrating Eq. (A1) we obtain the following formulas for the non-dimensional times $C\tau_{out}$ and $C\tau_{in}$ taken for a fluid circle to travel inward from $R(0)$ to r_u and from r_u to $R(t)$, respectively:

$$C\tau_{out} = \frac{A(0)}{a_u} - 1, \quad C\tau_{in} = \ln\frac{a_u}{A(t)} \tag{A4}$$

where $A(0) = \Gamma_a/f$ is the initial area. Generally τ_{out} is much larger than τ_{in} because a fluid area reduces linearly with time in the confluent region and declines exponentially in the CZ.

In summary, the total time τ for vortex formation directly from the Earth's rotation is

$$\tau = \frac{1}{C}\left(\frac{\Gamma_a}{f\pi r_u^2} - 1 + \ln\frac{r_u^2}{r_c^2}\right) \tag{A5}$$

where r_c is the core radius of the vortex. This formula underestimates the vortex-formation time because it ignores turbulent diffusion of angular momentum, which would slow and eventually stop the contraction of fluid circles near the axis, and also neglects losses of angular momentum to the ground.

For example, we can estimate from Eq. (A5) the time required for a strong tornado with a core radius of 100 m and a circulation 5×10^4 m^2 s^{-1} to form directly from the Earth's rotation underneath an updraft with a near-ground radius of 3 km. From Eq. (A2) we find that obtaining this much circulation requires contraction to 100 m radius of a fluid circle originally 13.1 km in radius. The initial radial and absolute tangential velocities on the fluid circle are -1.7 m s^{-1} and 0.6 m s^{-1}, respectively. For continual convergence of 5×10^{-3} s^{-1} within the convergence-zone radius of 3 km, and $1/f = 3$ h (the value at 40°N), τ =83 min (τ_{out} = 60 min and τ_{in} = 23 min) from

Eq. (A4). In the same radial-velocity field, a small, weak tornado with circulation 1.25×10^4 m^2 s^{-1} and core radius 50 m would take 40 min to form ($\tau_{out} = 13$ min and $\tau_{in} = 27$ min) from a fluid circle with an initial radius of 6.6 km.

Another illustration is provided by the passage of a tornado cyclone over a weather station at Newton, Kansas on 24 May 1962. The parent storm was four hours old at the time. From a trace of surface pressure (with a pressure deficit of 34 mb) and radar observations, Ward (1964) estimated maximum surface winds of 56 m s^{-1} at a radius of 1.6 km. The circulation is therefore 5.6×10^5 m^2 s^{-1}, which requires an initial fluid circle 44 km in radius if the formation mechanism is concentration of purely planetary vorticity. Even for a *large* convergence zones (radius 4.5 km) with *persistent* convergence of 5×10^{-3} s^{-1}, the estimated formation time of 5 h 22 min ($\tau_{out} = 315$ min and $\tau_{in} = 7$ min) is too long.

References

Adlerman, E.J., Droegemeier, K.K., Davies-Jones, R.P., 1999. A numerical simulation of cyclic mesocyclogenesis. J. Atmos. Sci. 56, 2045–2069.

Beck, J., Weiss, C., 2013. An assessment of low-level baroclinity and vorticity within a simulated supercell. Mon. Weather Rev. 141, 649–669.

Bluestein, H.B., 2013. Severe Convective Storms and Tornadoes. Springer (456 pp.).

Burgess, D.W., Lemon, L.R., 1990. Severe thunderstorm detection by radar. In: Atlas, D. (Ed.), Radar in Meteorology: Battan Memorial and 40th Anniversary Radar Conference. Amer. Meteor. Soc., pp. 619–656.

Dahl, J.M.L., Parker, M.D., Wicker, L.J., 2012. Uncertainties in trajectory calculations within near-surface mesocyclones of simulated supercells. Mon. Weather Rev. 140, 2959–2966.

Davies-Jones, R.P., 1982a. A new look at the vorticity equation with application to tornadogenesis. Preprints, Twelfth Conf. on Severe Local Storms. Amer. Meteor. Soc, San Antonio, TX, pp. 249–252.

Davies-Jones, R.P., 1982b. Observational and theoretical aspects of tornadogenesis. In: Bengtsson, L., Lighthill, J. (Eds.), Intense Atmospheric Vortices. Springer-Verlag, pp. 175–189.

Davies-Jones, R., 1984. Streamwise vorticity: the origin of updraft rotation in supercell storms. J. Atmos. Sci. 41, 2991–3006.

Davies-Jones, R., 1986. Tornado dynamics, In: Kessler, E. (Ed.), Thunderstorms Morphology and Dynamics, second ed. University of Oklahoma Press, pp. 197–236.

Davies-Jones, R., 2002. Linear and nonlinear propagation of supercell storms. J. Atmos. Sci. 59, 3178–3205.

Davies-Jones, R., 2004. Growth of circulation around supercell updrafts. J. Atmos. Sci. 61, 2863–2876.

Davies-Jones, R., 2006. Integrals of the vorticity equation. Part I: General three- and two-dimensional flows. J. Atmos. Sci. 63, 598–610.

Davies-Jones, R., 2008. Can a descending rain curtain in a supercell instigate tornadogenesis barotropically? J. Atmos. Sci. 65, 2469–2497.

Davies-Jones, R.P., Brooks, H.E., 1993. Mesocyclogenesis from a theoretical perspective. In: Church, C., Burgess, D., Doswell, C., Davies-Jones, R. (Eds.), The Tornado: Its Structure, Dynamics, Prediction, and Hazards, Geophys. Monogr. No. 79. Amer. Geophys. Union, pp. 105–114.

Davies-Jones, R.P., Golden, J.H., 1975. On the relation of electrical activity to tornadoes. J. Geophys. Res. 80, 1614–1616.

Davies-Jones, R.P., Kessler, E., 1974. Tornadoes. In: Hess, W.N. (Ed.), Weather and Climate Modification. John Wiley and Sons, New York, pp. 552–595.

Davies-Jones, R., Markowski, P., 2013. Lifting of ambient air by density currents in sheared environments. J. Atmos. Sci. 70, 1204–1215.

Davies-Jones, R.P., Burgess, D.W., Foster, M., 1990. Test of helicity as a tornado forecast parameter. In: *Preprints*. 16th Conf. Severe Local Storms, Kananaskis Provincial Park, Alberta, Amer. Meteor. Soc, pp. 588–592.

Davies-Jones, R.P., Trapp, R.J., Bluestein, H.B., 2001. Tornadoes and tornadic storms. In: Doswell, C. (Ed.), Severe Convective Storms, Meteor. Monogr. No. 50. Amer. Meteor. Soc., pp. 167–221.

Droegemeier, K.K., Lazarus, S.M., Davies-Jones, R., 1993. The influence of helicity on numerically modelled storms. Mon. Weather Rev. 121, 2005–2029.

Dutton, J.A., 1986. The Ceaseless Wind (Dover, 617 pp.).

Epifanio, C.C., Durran, D.R., 2002. Lee-vortex formation in free-slip stratified flow over ridges. Part II: mechanism of vorticity and PV production in nonlinear viscous wakes. J. Atmos. Sci. 59, 1166–1181.

Fiedler, B.H., Rotunno, R., 1986. A theory for the maximum windspeed in tornado-like vortices. J. Atmos. Sci. 43, 2328–2340.

Fujita, T.T., 1975. New evidence from April 3–4, 1974 tornadoes. Preprints, 9th Conf. Severe Local Storms, Norman, OK. Amer. Meteor. Soc., pp. 248–255.

Kis, A.K., Straka, J.M., Kanak, K.M., Davies-Jones, R.P., 2008. On the role of descending rain curtains in tornadogenesis. Extended Abstracts, 24th Conf. Severe Local Storms, Savannah, GA. Amer. Meteor. Soc. (14.5 A).

Klemp, J.B., 1987. Dynamics of tornadic thunderstorms. Annu. Rev. Fluid Mech. 19, 369–402.

Klemp, J.B., Wilhelmson, R.B., 1978. Simulations of right- and left-moving moving storms produced by storm splitting. J. Atmos. Sci. 35, 1097–1110.

Lewellen, W.S., 1976. Theoretical models of the tornado vortex. Proceedings, "A Symposium on Tornadoes: Assessment of Knowledge and Implications for Man". Texas Tech. Univ, Lubbock, pp. 107–143.

Lewellen, W.S., 1993. Tornado vortex theory. In: Church, C., Burgess, D., Doswell, C., Davies-Jones, R. (Eds.), The Tornado: Its Structure, Dynamics, Prediction, and Hazards. Geophys. Monogr., 79. Amer. Geophys. Union, pp. 19–39.

Lewellen, D.C., Lewellen, W.S., 2007. Near-surface intensification of tornado vortices. J. Atmos. Sci. 64, 2176–2194.

Lewellen, D.C., Lewellen, W.S., Xia, J., 2000. The influence of a local swirl ratio on tornado intensification near the surface. J. Atmos. Sci. 57, 527–544.

Lilly, D.K., 1969. Tornado Dynamics. NCAR Manuscript 69–117. National Center for Atmospheric Research, Boulder, Colorado.

Lilly, D.K., 1982. The development and maintenance of rotation in convective storms. In: Bengtsson, L., Lighthill, J. (Eds.), Intense Atmospheric Vortices. Springer-Verlag, pp. 149–160.

Markowski, P.M., 2002a. Mobile mesonet observations on 3 May 1999. Weather Forecast. 17, 430–444.

Markowski, P.M., 2002b. Hook echoes and rear-flank downdrafts: a review. Mon. Weather Rev. 130, 852–876.

Markowski, P.M., Richardson, Y.P., 2010. Mesoscale Meteorology in Midlatitudes. Wiley (430 pp.).

Markowski, P.M., Richardson, Y.P., 2014. The influence of environmental low-level shear and cold pools on tornadogenesis: insights from toy simulations. J. Atmos. Sci. (in press).

Markowski, P.M., Straka, J.M., Rasmussen, E.N., 1998. A preliminary investigation of the importance of helicity 'location' in the hodograph. Preprints, *19th Conf. on Severe Local Storms*. Amer. Meteor. Soc, Minneapolis, MN, pp. 230–233.

Markowski, P.M., Straka, J.M., Rasmussen, E.N., 2002. Direct surface thermodynamic observations within the rear-flank downdrafts of nontornadic and tornadic supercells. Mon. Weather Rev. 130, 1692–1721.

Markowski, P.M., Straka, J.M., Rasmussen, E.N., 2003. Tornadogenesis resulting from the transport of circulation by a downdraft: Idealized numerical simulations. J. Atmos. Sci. 60, 795–823.

Markowski, P., Richardson, Y., Marquis, J., Davies-Jones, R., Wurman, J., Kosiba, K., Robinson, P., Rasmussen, E., Dowell, D., 2012. The pretornadic phase of the Goshen County, Wyoming, supercell of 5 June 2009 intercepted by VORTEX2. Part II. Intensification of low-level rotation. Mon. Weather Rev. 140, 2916–2938.

Rasmussen, E.N., Straka, J.M., 2007. Evolution of low-level angular momentum in the 2 June 1995 Dimmitt, Texas, tornado cyclone. J. Atmos. Sci. 64, 1365–1378.

Rotunno, R., 1978. A note on the stability of a cylindrical vortex sheet. J. Fluid Mech. 87, 761–771.

Rotunno, R., 1986. Tornadoes and tornadogenesis. In: Ray, P.S. (Ed.), Mesoscale Meteorology and Forecasting. Amer. Meteor. Soc, pp. 414–436.

Rotunno, R., 2013. The fluid dynamics of tornadoes. Annu. Rev. Fluid Mech. 45, 59–84.

Rotunno, R., Klemp, J.B., 1982. The influence of the shear-induced pressure-gradient on thunderstorm motion. Mon. Weather Rev. 110, 136–151.

Rotunno, R., Klemp, J.B., 1985. On the rotation and propagation of simulated supercell thunderstorms. J. Atmos. Sci. 42, 271–292.

Simpson, J., 1982. Cumulus rotation. Model and observations of a waterspout-bearing cloud system. In: Bengtsson, L., Lighthill, J. (Eds.), Intense Atmospheric Vortices. Springer-Verlag, pp. 161–173.

Smith, R.K., Leslie, L.M., 1978. Tornadogenesis. Q. J. R. Meteorol. Soc. 104, 189–199.

Snow, J.T., Pauley, R.L., 1984. On the thermodynamic method for estimating tornado windspeeds. J. Clim. Appl. Meteorol. 23, 1465–1468.

Straka, J.M., Rasmussen, E.N., 1997. Towards improving microphysical parameterizations of conversion processes. J. Appl. Meteorol. 36, 896–902.

Trapp, R.J., Davies-Jones, R., 1997. Tornadogenesis with and without a dynamic pipe effect. J. Atmos. Sci. 54, 113–133.

Ward, N.B., 1964. The Newton, Kansas tornado cyclone of May 24, 1962. Proceedings of the 11th Weather Radar Conference, Boulder, Colorado. Amer. Meteor. Soc, Boston, MA, pp. 410–415.

Ward, N.B., 1972. The exploration of certain features of tornado dynamics using a laboratory model. J. Atmos. Sci. 29, 1194–1204.

Wicker, L.J., Wilhelmson, R.B., 1995. Simulation and analysis of tornado development and decay within a three-dimensional supercell thunderstorm. J. Atmos. Sci. 52, 2675–2703.